ACS Macro Letters

Letter

Cite This: ACS Macro Lett. 2018, 7, 1003−1009

pubs.acs.org/macroletters

Measurement of Cohesion and Adhesion of Semiconducting Polymers by Scratch Testing: Effect of Side-Chain Length and Degree of Polymerization

Daniel Rodriquez,[†] James G. Kohl,[‡] Pierre Morel,[§] Kyle Burrows,[§] Grégory Favaro,[⊥] Samuel E. Root,[†] Julian Ramírez,[†] Mohammad A. Alkhadra,[†] Cody W. Carpenter,[†] Zhuping Fei,[∥] Pierre Boufflet,[∥] Martin Heeney,[∥] and Darren J. Lipomi*[,†]

[†]Department of NanoEngineering, University of California−San Diego 9500 Gilman Drive, Mail Code 0448, La Jolla, California 92093-0448, United States

[‡]Department of Mechanical Engineering, Shiley-Marcos School of Engineering, University of San Diego, San Diego, California 92110-2492, United States

[∥]Department of Chemistry and Centre for Plastic Electronics, Imperial College London, Exhibition Road, London, SW7 2AZ, United Kingdom

[§]TriTec, Anton Paar USA, Inc., 10215 Timber Ridge Drive, Ashland, Virginia 23005, United States

[⊥]TriTec, Anton Paar SA, CH-2034 Peseux, Switzerland

Supporting Information

ABSTRACT: Most advantages of organic electronic materials are enabled by mechanical deformability, as flexible (and stretchable) devices made from these materials must be able to withstand roll-to-roll printing and survive mechanical insults from the external environment. Cohesion and adhesion are two properties that dictate the mechanical reliability of a flexible organic electronic device. In this paper, progressive-load scratch tests are used for the first time to correlate the cohesive and adhesive behavior of poly(3-alkylthiophenes) (P3ATs) with respect to two molecular parameters: length of the alkyl side chain and molecular weight. In contrast to metrological techniques based on buckling or pull testing of pseudofreestanding films, scratch tests reveal information about both the cohesive and adhesive properties of thin polymeric films from a single procedure. Our data show a decrease in cohesion and adhesion, that is, a decrease in overall mechanical robustness, with increasing length of the side chain. This behavior is likely due to increases in free volume and concomitant decreases in the glass transition temperature. In contrast, we observe increases in both the cohesion and adhesion with increasing molecular weight. This behavior is attributed to an increased density of entanglements with high molecular weight, which manifests as increased extensibility. These observations are consistent with the results of molecular dynamics simulations. Interestingly, the normal (applied) forces associated with cohesive and adhesive failure are directly proportional to the average degree of polymerization, as opposed to simply the molecular weight, as the length of the alkyl side chain increases the molecular weight without increasing the degree of polymerization.

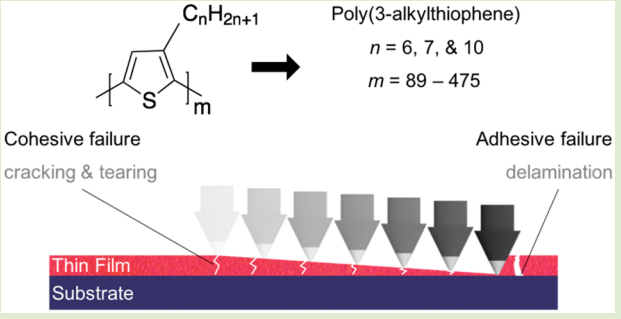

Organic electronic materials have applications ranging from ultrathin organic photovoltaic (OPV) devices[1,2] and organic field-effect transistors (OFETs)[3,4] to wearable sensors[5,6] and actuators.[7] The electronic properties of these materials, for example, as manifested in the efficiency of solar cells[8] and the charge-carrier mobility in thin-film transistors,[9] have improved dramatically, at least in devices fabricated at the laboratory scale. It is possible, however, that the performance at production scale could be limited by the mechanical reliability of a real device, which comprises multiple materials and interfaces.[10] In this study, we used progressive-load scratch testing for the first time to measure the cohesion and adhesion in thin films of poly(3-alkylthiophene)s (P3ATs) as functions of two parameters: length of the alkyl side chain and molecular weight (and thus the degree of polymerization). Strong cohesion can improve mechanical stability by increasing the resistance to the formation and propagation of fracture. (We use "cohesion" to refer to the resistance of the film to tearing under the applied load and the sum of the intermolecular forces, rather than specifically to the "cohesive fracture energy," an extensive property

Received: May 29, 2018
Accepted: July 27, 2018
Published: August 1, 2018

DOI: 10.1021/acsmacrolett.8b00412
ACS Macro Lett. 2018, 7, 1003−1009

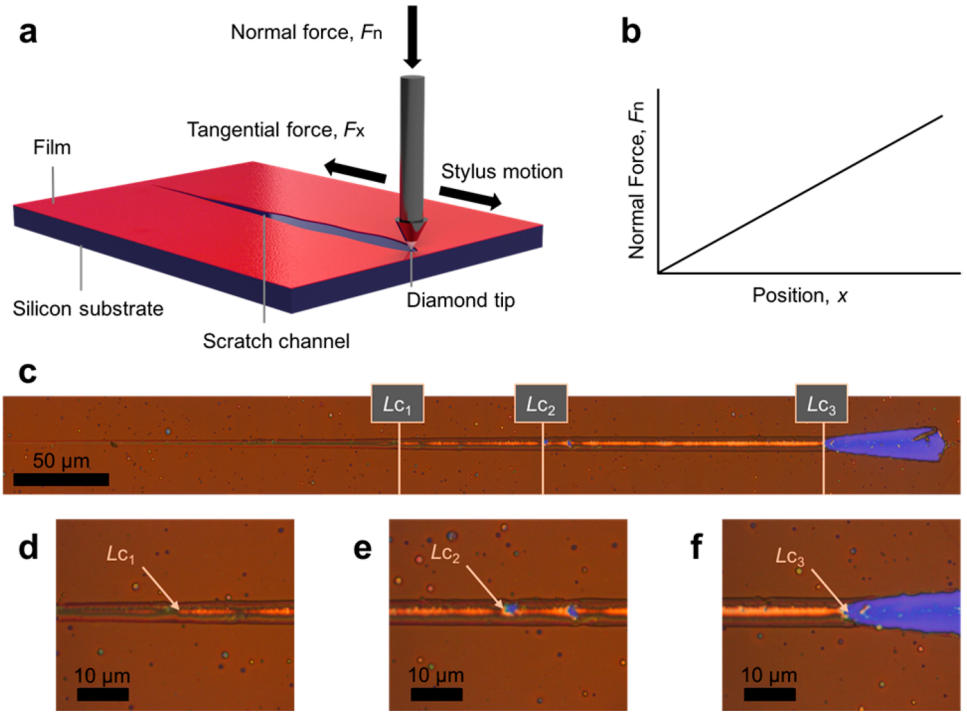

Figure 1. Scratch testing of thin films and coatings. (a) Schematic representation of a typical setup for scratch testing. (b) Profile of force vs position for a progressive-load scratch test. (c) Image of a scratch channel labeled with locations of critical failure, Lc_1, Lc_2, and Lc_3. (d) Magnified images of Lc_1, (e) Lc_2, and (f) Lc_3.

measured using the four-point bending[11] or double-cantilever beam test.[12]) Furthermore, since these devices are typically supported or encapsulated by a substrate, and composed of several layers, good adhesive strength is necessary to prevent delamination. Organic semiconductors, however, tend to exhibit poor adhesion as illustrated by recent studies on roll-to-roll printed OPV devices that determined the dominant mechanism of failure in these devices was delamination at the electrode−semiconductor interface.[12−14]

Scratch testing is an attractive method of characterizing the cohesion and adhesion of thin films on substrates, in a single test. The greatest strength of scratch testing is its practicality. Moreover, the sample used for testing can be made to isolate aspects of a real device: for example, the material of interest can be measured on realistic substrates, as opposed to on water or silicone rubber. During a scratch test, the initial response of the film to indentation is purely elastic.[15] As the force is increased, a critical load is reached that exceeds the elastic limit of the soft film and plastic deformation begins to occur (assuming the hardness of the indenter tip is much greater than that of the film).[15] Cohesive failure then occurs due to tensile stress behind the stylus tip and is observed as cracking or tearing in the film. Similarly, adhesive failure occurs due to compressive stress in front of the stylus tip, leading to delamination of the film by buckling or spallation. Schwarzer analyzed the stress distribution in scratch tests using the concept of the effective indenter and extended Hertzian theory.[16] In scratch tests both the cohesive and adhesive failure of thin films are thickness dependent, but saturate above a critical thickness (bulk value).[15] A prior study showed that cohesion and adhesion increased linearly with thickness for silicone elastomer coatings, until the bulk value was reached.[17] By assessing the type of crack propagation (i.e., tensile, conformal, Hertz) and spallation (i.e., buckling, compressive, gross) the mechanical failure mode (i.e., brittle vs ductile) may be identified.[18] Since scratch testing can characterize cohesive and adhesive behavior, as well as brittleness and ductility, it may be used as a complement or even replacement for existing methods of metrology.

We selected P3ATs as the model materials. P3ATs are the most commonly studied subset of conjugated polymers and have been central to the development of organic electronics.[19] The mechanical properties (elastic modulus, yield strength, ductility, and toughness),[20] electronic properties (charge-carrier mobility),[21] and thermal transitions[22] of P3ATs are well-known. Moreover, the quasi-living nature of the synthesis of P3ATs permits control over the molecular weight and dispersity, and the length of the alkyl side chain is similarly easy to control when preparing the monomer. We selected alkyl side chain lengths of n = 6, 7, and 10 since the glass transition temperatures (T_g) of these materials are around (n = 6, P3HT), below (n = 7, P3HpT), and well below (n = 10, P3DT) room temperature. Similarly, we chose molecular weights that ranged above and below the previously reported entanglement molecular weight of P3HT (35 kDa). To eliminate effects caused by large deviations in molecular weight, we selected dispersities in a narrow range.

A schematic illustration of a typical setup for scratch testing is depicted in Figure 1a. In a progressive-load scratch test, a stylus is dragged across the surface of a sample with an applied load that increases linearly with position, as described in Figure 1b. The location at which the film exhibits critical failure (Lc_i) and the corresponding normal force (Fn_i) are recorded during the experiment. The failure events are identified by the operator with assistance from optical microscopy, acoustic emission, and image analysis software.[23] The Lc_i associated with the failure of a film is a function of the adhesion between the film and the substrate, the thickness of the film, the rate of loading, the shape of the stylus tip, and the mechanical properties of both

DOI: 10.1021/acsmacrolett.8b00412
ACS Macro Lett. 2018, 7, 1003−1009

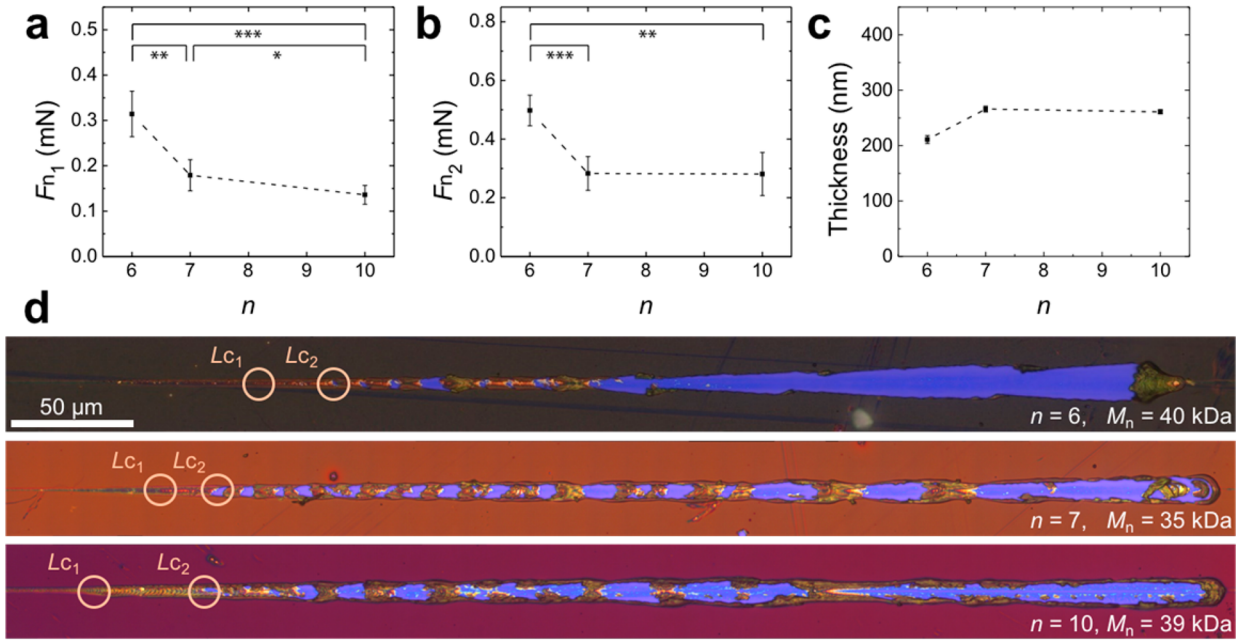

Figure 2. Results from scratch testing of P3ATs as a function of the length of the side chain *n*. (a, b) Normal forces recorded at each critical location, Lc_i. Data points represent mean ± s.d. (i = 5). *$P \leq 0.05$, **$P \leq 0.01$, ***$P \leq 0.001$, ****$P \leq 0.0001$. (c) Thickness measurements of each film under study. (d) Scratch channel images of each P3AT tested. Color variation in the samples arises from changes in *n*, which affect the optical behavior of the films.

the substrate and the film.[17,24] Additionally, surface treatments affect the adhesion of the films to a substrate (i.e., silanes or oxygen plasma). If these properties (thickness, loading rate, stylus tip, substrate, surface treatment) are held constant, however, Fn_i may be used as the basis for a comparative analysis of the films.[15] Typically, the applied force is recorded at three distinct positions which are indicative of critical failure, as shown in Figure 1c. Lc_1 is the location in the direction of displacement where the stylus first tears the surface of the film, but has not touched the substrate. In our tests, Lc_1 was identified by a change in the appearance of the film (from dark orange to bright orange) in the scratch channel which signaled tearing, Figure 1d. (An AFM image of this region of the scratch channel is given in Figure S1.) The normal force measured at this position, Fn_1, is a measure of the resistance of the sample to cohesive failure. The region to the left of Lc_1 is the residual penetration depth of the stylus, which is due to plastic deformation of the film. Lc_2 is the location at which the stylus scratches through the sample completely and contacts the substrate; this position signals the onset of adhesive failure, Figure 1e. Finally, Lc_3 is the position at which gross delamination begins to occur, Figure 1f. The forces corresponding to positions Lc_2 and Lc_3 are used to compare the adhesion of materials to substrates.

Results from the scratch testing of P3ATs, Figure 2a, show a decrease in cohesion as a function of the length of the alkyl side chain *n* (probability value (P) ≤ 0.001 between n = 6 and 10). The effect of *n* on the mechanical properties of thin films of P3ATs was previously examined both experimentally[25] and computationally:[26] with increasing *n*, the ductility increases, whereas the elastic modulus decreases. This effect was a manifestation of the glass transition temperature, T_g, changing from near room temperature to well below it as *n* changed from 6 to 7.[25] The decrease in the T_g is a result of increased free volume in the polymer film with increasing *n*. Since van der Waals forces are dependent on the inverse sixth power of interchain distance, small changes in separation between the main chains (decreased density) will produce large decreases in the intermolecular forces and decreased cohesion.[27] To examine the effect of increasing *n* on aggregation behavior, which is known to influence mechanical properties,[28] we obtained UV/vis spectra. We found that an increase in *n* corresponded to a decrease in the conjugation length and the fraction of aggregates in the films, as determined using the weakly interacting H-aggregate model[29−31] (Figure S2 and Table S1). Decreased adhesion of P3ATs with increasing *n* ($P \leq 0.01$ between n = 6 and 10), as shown in Figure 2b, is also consistent with reduced density (the Hamaker constant, which characterizes the adhesion between solids, is proportional to density). A prior study has shown that the surface energy of P3AT thin films decreased with *n*, as measured by an increase in water contact angle.[25]

The normal forces recorded at the beginning of gross delamination (Fn_3) did not exhibit a clearly observable trend and contained a considerable amount of error. The error was due to ambiguity in the labeling of Fn_3 for n = 7 and 10. Therefore, we did not consider measurements of Fn_3 in our analysis. Upon visual inspection, however, it appears that films of n = 7 and 10 exhibit lower adhesive strength than n = 6 (the films fail adhesively further to the left). Figure 2c plots the thickness of each film as a function of *n*. Figure 2d shows the scratch channel for each of the P3ATs tested as a function of *n*. The images qualitatively show a decrease in the normal force required to induce failure by observing that the initiation of Lc_1 and Lc_2 occurred earlier in the scratch test (Fn_i increased linearly).

It is well-known that the molecular weight of conjugated polymers strongly influence the density of entanglements and, therefore, the mechanical properties.[20,22] We thus performed scratch tests on P3HT having a range of M_n. The results show an increase in the cohesion as a function of M_n, Figure 3a ($P \leq$ 0.0001 between M_n = 15 and 80 kDa). By way of comparison, critical forces measured for the P3HT (80 kDa) sample correspond to the following data obtained by tensile testing: modulus, 0.27 GPa; toughness, 13.17 MJ m^{-3}; tensile strength, 17.1 MPa,

DOI: 10.1021/acsmacrolett.8b00412
ACS Macro Lett. 2018, 7, 1003−1009

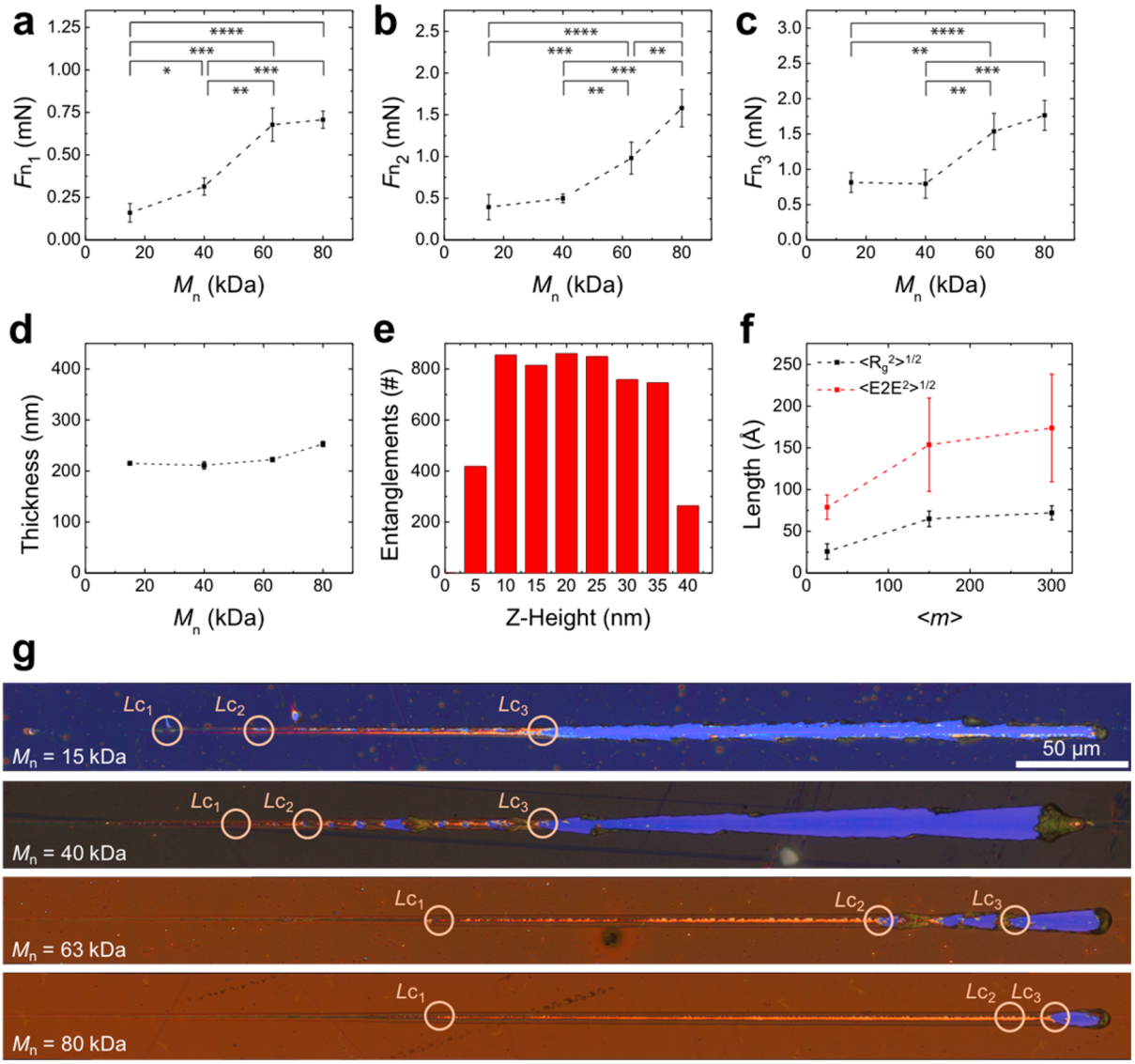

Figure 3. Scratch testing results for P3HT as a function of M_n. (a–c) Normal forces recorded at each critical location, Lc_i. Data points represent means ± s.d. (i = 5). *$P \leq 0.05$, **$P \leq 0.01$, ***$P \leq 0.001$, ****$P \leq 0.0001$. (d) Thickness measurements of each M_n tested. (e) Coarse-grained molecular dynamics estimation of the number of "entanglements", calculated as the number of interior kinks per chain,[26] as a function of Z-height in a 40 nm P3HT thin film (300 repeat units). (f) Coarse-grained molecular dynamics predictions of the RMS radius of gyration ($\langle R_g^2 \rangle^{1/2}$) and the RMS end-to-end distance ($\langle E2E^2 \rangle^{1/2}$) for three representative chain lengths. (g) Scratch channel images of each M_n tested. Color differences between the samples arise from changes in aggregation behavior with increasing M_n, which affect the optical behavior of the films, see Figure S2 and Table S1.

Table 1.[20] For regioregular P3HT, increases in M_n lead to physical linking of polymer chains (entanglements) and tie molecules that traverse multiple crystallites, which increase the connectivity between chains.[32] This effect is magnified once the polymer length exceeds the entanglement molecular weight. It thus has a direct impact on the cohesive strength of conjugated polymers as it raises the energy required for chain disentanglement and chain pullout.[11] Similar results showing an increase in the cohesive strength of P3HT:fullerene bulk heterojunction films as a function of M_n have been reported.[11] Additionally, prior studies have shown that extensibility and toughness increase with increasing molecular weight of P3HT, Table 1.[20,22]

It has been hypothesized that the M_n of a polymer may have a significant impact on the adhesion of the material to a substrate.[33] Our results support this premise as the adhesion of P3HT increased as a function of M_n, shown in Figure 3b,c

Table 1. Tabulated Values of the Mechanical Properties of P3HT in a Range of Molecular Weights As Determined by Tensile Testing[a]

mechanical properties of P3HT				
M_n (kDa)	tensile modulus (GPa)	strain at fracture (%)	toughness (MJ/m^3)	tensile strength (MPa)
15	0.203 ± 0.014	4.5 ± 0.3	0.14 ± 0.01	4.5 ± 0.3
40	0.263 ± 0.015	13.0 ± 1.2	0.99 ± 0.08	10.5 ± 0.5
63	0.261 ± 0.020	58.7 ± 6.5	6.80 ± 0.78	12.6 ± 0.2
80	0.270 ± 0.012	95.6 ± 7.7	13.17 ± 0.97	17.1 ± 0.6

[a]The tests were conducted in a prior study.[20]

($P \leq 0.0001$ between M_n = 15 and 80 kDa). Since the thickness of the samples was held relatively constant, Figure 3d, thickness dependence may be eliminated as the dominating factor for the

DOI: 10.1021/acsmacrolett.8b00412
ACS Macro Lett. 2018, 7, 1003–1009

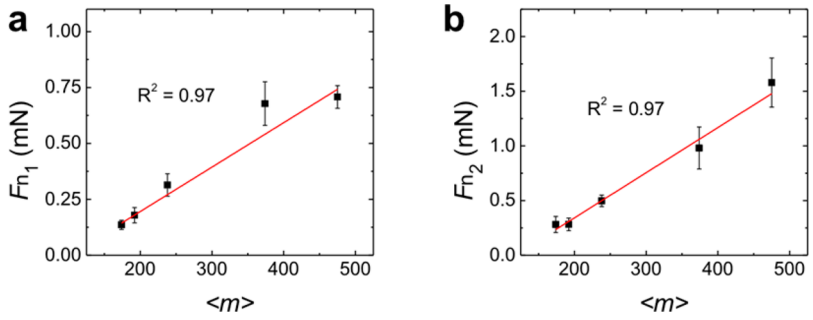

Figure 4. Plots showing the linear relationship between average degree of polymerization $\langle m \rangle$ and the force required for failure: (a) Fn_1 and (b) Fn_2 vs $\langle m \rangle$.

observed increase in Fn_2 and Fn_3. The increase in adhesion may be explained, in part, by the presence of a "liquid-like" skin layer near the free surfaces of the polymer films which dissipates stress. In this region, the polymer chains are highly mobile and less entangled than in the bulk. To simulate the number of entanglements as they vary with the Z-height of a thin film we performed coarse-grained molecular dynamics using a well-established model for P3HT that contains three coarse-grained sites per monomer,[34] Figure 3e. The number of entanglements is estimated from the intersections of the primitive paths of the polymer chains, that is, the number of interior kinks per chain.[26] The results show that for a 40 nm thin film of P3HT (300 repeat units), the density of entanglements is initially low and then increases sharply 5 nm into the film (on both the top and bottom surfaces). For sufficiently thin films, the skin layer has a thickness on the same order of magnitude as the length of individual polymer chains. Using the same model, the predicted trend for the RMS radius of gyration $\langle R_g^2 \rangle^{1/2}$ and RMS end-to-end distance $\langle E2E^2 \rangle^{1/2}$ as a function of the average number of repeat units in the polymer chain $\langle m \rangle$ is shown in Figure 3f. Our results suggest that, for a film thickness of 120 nm, the skin region comprises approximately 10% of the total film thickness for P3HT with low M_n and approximately 30% of the total film thickness for P3HT with high M_n. For high M_n polymers, it can be expected that the larger volume of the skin layer will lead to a greater capacity to dissipate mechanical energy during adhesive failure, resulting in increased adhesion.

It should also be noted that all the results from scratch testing involve some level of cooperativity between cohesive strength and adhesion. During a scratch test, for a film to fail adhesively, it must first fail cohesively by cracking through the thickness of the film. The initiation and propagation of such a crack will lead to early adhesive failure by gross delamination, as seen in the low M_n P3HT film, Figure 3g. In high M_n samples, however, ductility increases and crack propagation is hindered by the plastic dissipation zone, a region near the crack tip that dissipates energy through plastic deformation.[35] It is then reasonable to assume that any observed increase in adhesion (Fn_3 and Lc_3) is partly a consequence of the increased cohesive strength of P3HT films with greater M_n, and their ability to dissipate mechanical energy.

Figure 4a,b plots the normal force associated with cohesion and adhesion as a function of the average number of repeat units $\langle m \rangle$. We chose $\langle m \rangle$ for our analysis, as opposed to M_n, since two polymers of the same M_n may have different degrees of polymerization, depending on the mass of the monomer (i.e., P3HT vs P3DT). Interestingly, there is a linear correlation between $\langle m \rangle$ and the forces required for failure for all polymers above the entanglement molecular weight, regardless of n. We note that one data point was excluded, P3HT (M_n = 15 kDa), since this sample was below the entanglement molecular weight. In P3ATs, the length of the side chain seems to play a secondary role to the length of the main chain once the entanglement molecular weight has been surpassed. This is a seemingly desirable result since the charge-carrier mobility of P3HT generally improves with increasing M_n and plateaus once the entanglement M_n is surpassed.[36] The increase in electronic performance arises from favorable changes in morphology in the films. At low M_n, the polymer chains exist as noninterconnected chain extended crystals and charge transport is hindered by grain boundaries that create energetic trap states.[22] At high M_n, the polymer chains exhibit a larger degree of self-folding and tie molecules that connect crystalline regions of the polymer film; this morphology results in improved charge transport.[21,22,36,37]

These results suggest that progressive-load scratch testing has considerable value in measuring the cohesion and adhesion of conjugated polymers. In particular, measurements of P3ATs as a function of the length of the side chain n and P3HT in a range of M_n have shown that cohesion and adhesion decreased as a function of n for P3ATs and increased with M_n for P3HT. When the results are plotted as a function of repeat units $\langle m \rangle$, for all polymers above the entanglement molecular weight, we observed a linear relationship between $\langle m \rangle$ and the associated normal forces of failure. This work demonstrates the practicality of scratch testing as a method of characterizing the cohesive and adhesive behavior of organic semiconductors. Our findings could inform the design of conjugated polymers that exhibit greater mechanical reliability in organic electronic devices.

■ ASSOCIATED CONTENT

Supporting Information

The Supporting Information is available free of charge on the ACS Publications website at DOI: 10.1021/acsmacrolett.8b00412.

Experimental methods, UV/vis absorption spectra, H-aggregate analysis, and AFM images of a scratch channel (PDF).

■ AUTHOR INFORMATION

Corresponding Author

*E-mail: dlipomi@eng.ucsd.edu.

ORCID

Martin Heeney: 0000-0001-6879-5020

Darren J. Lipomi: 0000-0002-5808-7765

Notes

The authors declare no competing financial interest.

DOI: 10.1021/acsmacrolett.8b00412
ACS Macro Lett. 2018, 7, 1003−1009

■ ACKNOWLEDGMENTS

This research was supported primarily by the Air Force Office of Scientific Research (AFOSR) Grant No. FA9550-16-1-0220. D.R. and J.R. acknowledge support provided by the National Science Foundation Graduate Research Fellowship Program under Grant No. DGE-1144086. Computational resources to support this work were provided by the Extreme Science and Engineering Discovery Environment (XSEDE) Program through the National Science Foundation Grant No. ACI-1053575.

■ REFERENCES

(1) Kim, T.; Kim, J.-H.; Kang, T. E.; Lee, C.; Kang, H.; Shin, M.; Wang, C.; Ma, B.; Jeong, U.; Kim, T.-S.; Kim, B. J. Flexible, Highly Efficient All-Polymer Solar Cells. *Nat. Commun.* **2015**, *6* (1), 8547.

(2) Jean, J.; Wang, A.; Bulović, V. In Situ Vapor-Deposited Parylene Substrates for Ultra-Thin, Lightweight Organic Solar Cells. *Org. Electron.* **2016**, *31*, 120−126.

(3) Young Oh, J.; Rondeau-Gagné, S.; Chiu, Y.-C.; Chortos, A.; Lissel, F.; Nathan Wang, G.-J.; Schroeder, B. C.; Kurosawa, T.; Lopez, J.; Katsumata, T.; Xu, J.; Zhu, C.; Gu, X.; Bae, W.-G.; Kim, Y.; Jin, L.; Won Chung, J.; B-H Tok, J.; Bao, Z. Intrinsically Stretchable and Healable Semiconducting Polymer for Organic Transistors. *Nature* **2016**, *539* (7629), 411−415.

(4) Kaltenbrunner, M.; Sekitani, T.; Reeder, J.; Yokota, T.; Kuribara, K.; Tokuhara, T.; Drack, M.; Schwödiauer, R.; Graz, I.; Bauer-Gogonea, S.; Bauer, S.; Someya, T. An Ultra-Lightweight Design for Imperceptible Plastic Electronics. *Nature* **2013**, *499* (7459), 458−463.

(5) Roh, E.; Hwang, B.; Kim, D.; Kim, B.; Lee, N. Stretchable, Transparent, Ultrasensitive, and Patchable Strain Sensor for Human - Machine Interfaces Comprising a Nanohybrid of Carbon Sensor and Conductive Elastomers. *ACS Nano* **2015**, *9* (6), 6252−6261.

(6) Bihar, E.; Roberts, T.; Ismailova, E.; Saadaoui, M.; Isik, M.; Sanchez-Sanchez, A.; Mecerreyes, D.; Hervé, T.; De Graaf, J. B.; Malliaras, G. G. Fully Printed Electrodes on Stretchable Textiles for Long-Term Electrophysiology. *Adv. Mater. Technol.* **2017**, *2*, 1600251.

(7) Lim, S.; Son, D.; Kim, J.; Lee, Y. B.; Song, J. K.; Choi, S.; Lee, D. J.; Kim, J. H.; Lee, M.; Hyeon, T.; Kim, D. H. Transparent and Stretchable Interactive Human Machine Interface Based on Patterned Graphene Heterostructures. *Adv. Funct. Mater.* **2015**, *25* (3), 375−383.

(8) Huang, J.; Wang, H.; Yan, K.; Zhang, X.; Chen, H.; Li, C. Z.; Yu, J. Highly Efficient Organic Solar Cells Consisting of Double Bulk Heterojunction Layers. *Adv. Mater.* **2017**, *29* (19), 1−9.

(9) Liu, J.; Dong, H.; Wang, Z.; Ji, D.; Cheng, C.; Geng, H.; Zhang, H.; Zhen, Y.; Jiang, L.; Fu, H.; Bo, Z.; Chen, W.; Shuai, Z.; Hu, W. Thin Film Field-Effect Transistors of 2,6-Diphenyl Anthracene (DPA). *Chem. Commun.* **2015**, *51* (59), 11777−11779.

(10) Root, S. E.; Savagatrup, S.; Printz, A. D.; Rodriquez, D.; Lipomi, D. J. Mechanical Properties of Organic Semiconductors for Stretchable, Highly Flexible, and Mechanically Robust Electronics. *Chem. Rev.* **2017**, *117* (9), 6467−6499.

(11) Bruner, C.; Dauskardt, R. Role of Molecular Weight on the Mechanical Device Properties of Organic Polymer Solar Cells. *Macromolecules* **2014**, *47*, 1117−1121.

(12) Dupont, S. R.; Oliver, M.; Krebs, F. C.; Dauskardt, R. H. Interlayer Adhesion in Roll-to-Roll Processed Flexible Inverted Polymer Solar Cells. *Sol. Energy Mater. Sol. Cells* **2012**, *97*, 171−175.

(13) Finn, M.; Martens, C. J.; Zaretski, A. V.; Roth, B.; Søndergaard, R. R.; Krebs, F. C.; Lipomi, D. J. Mechanical Stability of Roll-to-Roll Printed Solar Cells under Cyclic Bending and Torsion. *Sol. Energy Mater. Sol. Cells* **2018**, *174* (June), 7−15.

(14) Brand, V.; Bruner, C.; Dauskardt, R. H. Cohesion and Device Reliability in Organic Bulk Heterojunction Photovoltaic Cells. *Sol. Energy Mater. Sol. Cells* **2012**, *99*, 182−189.

(15) Benjamin, P.; Weaver, C. Measurement of Adhesion of Thin Films. *Proc. R. Soc. London, Ser. A* **1960**, *254* (1277), 163−176.

(16) Schwarzer, N. Completely Analytical Tools for the Next Generation of Surface and Coating Optimization. *Coatings* **2014**, *4* (2), 253−281.

(17) Kohl, J. G.; Singer, I. L.; Schwarzer, N.; Yu, V. Y. Effect of Bond Coat Modulus on the Durability of Silicone Duplex Coatings. *Prog. Org. Coat.* **2006**, *56* (2−3), 220−226.

(18) Tomastik, J.; Ctvrtlik, R. Nanoscratch Test — A Tool for Evaluation of Cohesive and Adhesive Properties of Thin Films and Coatings. *EPJ Web Conf.* **2013**, *48*, 00027.

(19) Kleinschmidt, A. T.; Root, S. E.; Lipomi, D. J. Poly(3-Hexylthiophene) (P3HT): Fruit Fly or Outlier in Organic Solar Cell Research? *J. Mater. Chem. A* **2017**, *5* (23), 11396−11400.

(20) Rodriquez, D.; Kim, J.-H.; Root, S. E.; Fei, Z.; Boufflet, P.; Heeney, M.; Kim, T.-S.; Lipomi, D. J. Comparison of Methods for Determining the Mechanical Properties of Semiconducting Polymer Films for Stretchable Electronics. *ACS Appl. Mater. Interfaces* **2017**, *9* (10), 8855−8862.

(21) Kline, R. J.; McGehee, M. D.; Kadnikova, E. N.; Liu, J.; Frechet, J. M. J. Controlling the Field-Effect Mobility of Regioregular Polythiophene by Changing the Molecular Weight. *Adv. Mater.* **2003**, *15* (18), 1519−1522.

(22) Koch, F. P. V.; Rivnay, J.; Foster, S.; Müller, C.; Downing, J. M.; Buchaca-Domingo, E.; Westacott, P.; Yu, L.; Yuan, M.; Baklar, M.; Fei, Z.; Luscombe, C.; McLachlan, M. A.; Heeney, M.; Rumbles, G.; Silva, C.; Salleo, A.; Nelson, J.; Smith, P.; Stingelin, N. The Impact of Molecular Weight on Microstructure and Charge Transport in Semicrystalline Polymer Semiconductors-Poly(3-Hexylthiophene), a Model Study. *Prog. Polym. Sci.* **2013**, *38* (12), 1978−1989.

(23) Sekler, J.; Steinmann, P. A.; Hintermann, H. E. The Scratch Test: Different Critical Load Determination Techniques. *Surf. Coat. Technol.* **1988**, *36* (1−2), 519−529.

(24) Kohl, J. G.; Randall, N. X.; Schwarzer, N.; Ngo, T. T.; Shockley, M. J.; Nair, R. P. An Investigation of Scratch Testing of Silicone Elastomer Coatings with a Thickness Gradient. *J. Appl. Polym. Sci.* **2012**, *124*, 2978−2986.

(25) Savagatrup, S.; Makaram, A. S.; Burke, D. J.; Lipomi, D. J. Mechanical Properties of Conjugated Polymers and Polymer-Fullerene Composites as a Function of Molecular Structure. *Adv. Funct. Mater.* **2014**, *24* (8), 1169−1181.

(26) Root, S. E.; Savagatrup, S.; Pais, C. J.; Arya, G.; Lipomi, D. J. Predicting the Mechanical Properties of Organic Semiconductors Using Coarse-Grained Molecular Dynamics Simulations. *Macromolecules* **2016**, *49* (7), 2886−2894.

(27) Jenekhe, S. A.; Roberts, M. F. Effects of Intermolecular Forces on the Glass Transition of Polymers. *Macromolecules* **1993**, *26* (18), 4981−4983.

(28) Awartani, O.; Lemanski, B. I.; Ro, H. W.; Richter, L. J.; DeLongchamp, D. M.; O'Connor, B. T. Correlating Stiffness, Ductility, and Morphology of Polymer:Fullerene Films for Solar Cell Applications. *Adv. Energy Mater.* **2013**, *3* (3), 399−406.

(29) Clark, J.; Chang, J. F.; Spano, F. C.; Friend, R. H.; Silva, C. Determining Exciton Bandwidth and Film Microstructure in Polythiophene Films Using Linear Absorption Spectroscopy. *Appl. Phys. Lett.* **2009**, *94* (16), 163306.

(30) Siddiqui, S.; Spano, F. C. H- and J-Aggregates of Conjugated Polymers and Oligomers. *Chem. Phys. Lett.* **1999**, *308* (1−2), 99−105.

(31) Spano, F. C. Modeling Disorder in Polymer Aggregates: The Optical Spectroscopy of Regioregular Poly(3-Hexylthiophene) Thin Films. *J. Chem. Phys.* **2005**, *122* (23), 234701.

(32) Brinkmann, M.; Rannou, P. Molecular Weight Dependence of Chain Packing and Semicrystalline Structure in Oriented Films of Regioregular Poly(3-Hexylthiophene) Revealed by High-Resolution Transmission Electron Microscopy. *Macromolecules* **2009**, *42* (4), 1125−1130.

(33) Choi, G. Y.; Zurawsky, W.; Ulman, A. Molecular Weight Effects in Adhesion. *Langmuir* **1999**, *15* (24), 8447−8450.

(34) Huang, D. M.; Faller, R.; Do, K.; Moul, A. J. Coarse-Grained Computer Simulations of Polymer/Fullerene Bulk Heterojunctions

DOI: 10.1021/acsmacrolett.8b00412
ACS Macro Lett. 2018, 7, 1003−1009

for Organic Photovoltaic Applications. *J. Chem. Theory Comput.* **2010**, *6*, 526−537.
(35) Alkhadra, M. A.; Root, S. E.; Hilby, K. M.; Rodriquez, D.; Sugiyama, F.; Lipomi, D. J. Quantifying the Fracture Behavior of Brittle and Ductile Thin Films of Semiconducting Polymers. *Chem. Mater.* **2017**, *29*, 10139−10149.
(36) Noriega, R.; Rivnay, J.; Vandewal, K.; Koch, F. P. V; Stingelin, N.; Smith, P.; Toney, M. F.; Salleo, A. A General Relationship between Disorder, Aggregation and Charge Transport in Conjugated Polymers. *Nat. Mater.* **2013**, *12* (11), 1038−1044.
(37) Kline, R. J.; Mcgehee, M. D.; Kadnikova, E. N.; Liu, J.; Frechet, J. M. J.; Toney, M. F. The Dependence of Regioregular Poly (3-Hexylthiophene) Film Morphology and Field-Effect Mobility on Molecular Weight. *Macromolecules* **2005**, *38* (December), 3312−3319.

DOI: 10.1021/acsmacrolett.8b00412
ACS Macro Lett. 2018, 7, 1003−1009